Magnetism-mediated transition between crystalline and higher-order topological phases in NpSb

Ning Mao,[1] Xiangting Hu,[1] Hao Wang,[1] Ying Dai,[1,*] Baibiao Huang,[1] Yuriy Mokrousov,[2,3] and Chengwang Niu[1,†]

[1]*School of Physics, State Key Laboratory of Crystal Materials, Shandong University, Jinan 250100, China*

[2]*Peter Grünberg Institut and Institute for Advanced Simulation, Forschungszentrum Jülich and JARA, 52425 Jülich, Germany*

[3]*Institute of Physics, Johannes Gutenberg University Mainz, 55099 Mainz, Germany*

(Received 26 January 2021; accepted 12 May 2021; published 24 May 2021)

Merging the fields of topology and magnetism expands the scope of fundamental quantum phenomena with novel functionalities for topological spintronics enormously. Here, we theoretically demonstrate that ferromagnetism provides an efficient means to achieve a topological switching between crystalline and higher-order topological insulator phases in two dimensions. Using a tight-binding model and first-principles calculations, we identify layered NpSb as a long-awaited two-dimensional topological crystalline insulator with intrinsic ferromagnetic order with a band gap which is as large as 220 meV. We show that when $\mathcal{M}_z$ symmetry is preserved for the out of plane magnetization of this material, it exhibits a pair of gapless edge states along all boundaries and carries a nonzero mirror Chern number $\mathcal{C}_{\mathcal{M}} = 1$. Remarkably, when rotating the magnetization into the plane a higher-order topological insulator phase with a parity-based invariant $\nu_{2D} = 1$ is achieved, and in-gap topological corner states emerge. Our results pave the way to understanding and engineering topological insulating states in two-dimensional ferromagnets.

DOI: 10.1103/PhysRevB.103.195152

I. INTRODUCTION

Topological crystalline insulators (TCIs), characterized by robust surface/edge states that emerge due to the crystalline symmetries, such as mirrors or rotations [1–5], give rise to unusual physical phenomena and even inspire novel families of topological spintronic devices [6–9]. In solids, TCIs can exist in two-dimensional (2D) and three-dimensional (3D) crystals regardless of time-reversal symmetry ($\mathcal{T}$), i.e., in both nonmagnetic and magnetic compounds [1,10]. However, following its first theoretical prediction and experimental confirmation in 3D nonmagnetic SnTe, TCIs were addressed mainly in nonmagnetic compounds and have yet to be synthesized experimentally in two dimensions [2,11–20]. Interestingly, the unique interplay of magnetism with 2D TCIs provides a playground for the complex interplay between magnetism, electronic correlations, and topological orders, realizing a rich set of exotic quantum states, such as quantum anomalous Hall effects, mixed Weyl semimetals, and topological nodal-line semimetals [21–24]. Indeed, a blend of topology and magnetism has attracted intensive attention that is currently maturing into a distinct burgeoning research field of condensed-matter physics [25–36]. Despite recent successes along this path, however, a 2D TCI with intrinsic magnetic order has still not been observed. Therefore, the search for 2D magnetic TCIs is highly desirable for both the fundamental understanding and future applications of 2D topological magnets.

On the other hand, theoretical advances in the domain of crystalline symmetry-protected topological states and bulk-boundary correspondence have greatly expanded the topological classification of band insulators, culminating in a recent discovery of so-called higher-order topological insulators (HOTIs) [37,38]. In contrast to typical d-dimensional TIs and/or TCIs, which host conducting $(d-1)$-dimensional boundary states [6–9], the gapless topological states of HOTIs appear in a lower codimension as the corner or hinge states in 2D and 3D, respectively, while their respective edges and surfaces are gapped [37,38]. Recently, a tremendous effort is being invested in unraveling the properties of HOTIs [39–50], which has started to reach out to the realm of 2D magnetism [51,52]. However, the material realization of 2D magnetic HOTIs is so far limited to the case of Bi/EuO heterostructure [52], while a realistic intrinsic magnetic 2D HOTI is still not known and the underlying physics of the formation of 2D magnetic HOTIs remains elusive.

In this work, we theoretically predict ferromagnetic NpSb monolayer as a realistic ferromagnet that can be either a 2D TCI or a 2D HOTI, depending on the direction of the magnetization. We thus predict that it is possible to realize a topological phase transition between a TCI and a HOTI state in the same material by invoking magnetic symmetries into the topological analysis. Our analysis shows that when the magnetization of ferromagnetic (FM) NpSb points out of the plane of the film (along z), it resides in a 2D TCI phase with gapless edge states emerging at all boundaries as a result of $\mathcal{M}_z$ mirror symmetry. For certain directions of the in-plane magnetization, $\mathcal{M}_z$ is broken but other mirror symmetries, such as $\mathcal{M}_{xy}$, can survive, which guarantees the emergence of topological corner states and nonzero winding number. The feasibility of attaining both the 2D FM TCI and FM HOTI is further understood based on a four-band tight-binding model. Our results not only provide an ideal platform to achieve both FM TCI and FM HOTI states in the same material but

*daiy60@sdu.edu.cn
†c.niu@sdu.edu.cn

may also put forward potential applications in topological spintronics.

II. MODEL HAMILTONIAN

In many magnetic 2D (in the xy plane) systems the $\mathcal{M}_z$ symmetry of reflection with respect to the xy plane is preserved when the magnetization points out of the plane (along z), which provides a recipe to define the mirror Chern number and achieve a TCI state. When the magnetization direction is varied, $\mathcal{M}_z$ symmetry is naturally broken and $(d-1)$-dimensional edge states become gapped. However, as we will show below, for certain directions of the magnetization other mirror symmetries are restored which results in the emergence of topologically protected corner states, i.e., $(d-2)$-dimensional boundary modes, appearing inside the band gap of the bulk and $(d-1)$-dimensional edges, thus manifesting the formation of magnetic HOTI state. To show this clearly from simple arguments, we start from a four-band tight-binding model for the 2D square lattice, as sketched in Fig. 1(a), with the Hamiltonian that can be expressed as $H = H_0 + H_B$ with

$$H_0 = [(m - t(\cos k_x + \cos k_y)]\tau_z - \lambda(\sin k_x \sigma_x + \sin k_y \sigma_y)\tau_x,$$
$$H_B = B\sigma_x \sin\theta\cos\varphi + B\sigma_y \sin\theta \sin\varphi + B\sigma_z \cos\theta. \quad (1)$$

Here, the onsite energy, the magnitude of the nearest-neighbor hopping, and the strength of spin-orbit coupling (SOC) correspond to parameters m, t, and λ, respectively. σ and τ are the vectors of spin and suborbital Pauli matrices. The FM order is represented by the Zeeman term H_B with an amplitude of exchange field given by B and the magnetization direction defined by spherical angles θ and φ. For $B = 0$, the model system possesses four flavors of symmetries: chiral symmetry $\mathcal{C}$ [50], time-reversal symmetry $\mathcal{T}$, inversion symmetry $\mathcal{P}$, and mirror symmetries $\mathcal{M}_z$ $(z \to -z)$, $\mathcal{M}_x$ $(x \to -x)$, $\mathcal{M}_y$ $(y \to -y)$, $\mathcal{M}_{xy}$ $(x \to -y, y \to -x)$, and $\mathcal{M}_{x\bar{y}}$ $(x \to y, y \to x)$, represented as $\mathcal{C} = \tau_x$, $\mathcal{T} = i\sigma_y$, $\mathcal{P} = \tau_z$, $\mathcal{M}_z = i\tau_z\sigma_z$, $\mathcal{M}_x = i\sigma_x$, $\mathcal{M}_y = i\sigma_y$, $\mathcal{M}_{xy} = i\sqrt{2}/2(\sigma_x + \sigma_y)$, and $\mathcal{M}_{x\bar{y}} = i\sqrt{2}/2(\sigma_x - \sigma_y)$. With a set of parameters that capture the band inversion ($m = 1.5t$ and $\lambda = t$) the system becomes a dual TI [53].

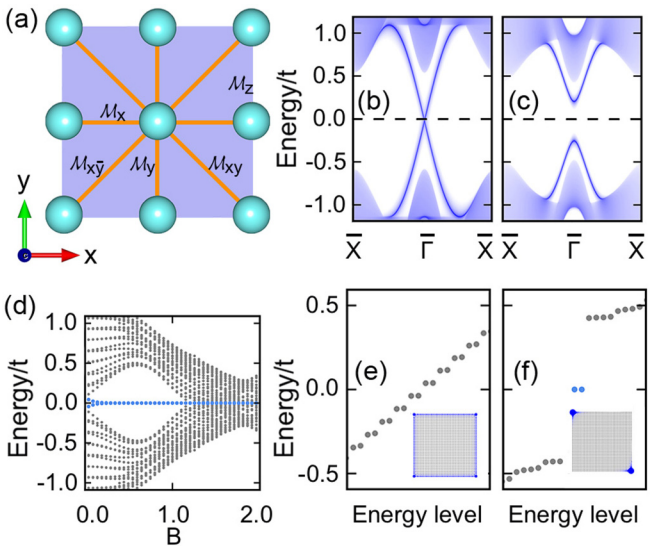

FIG. 1. (a) Sketch of a two-dimensional (2D) square lattice, in which the mirror symmetries depend sensitively on the magnetization direction. The shaded area indicates the mirror symmetry $\mathcal{M}_z$, and the solid lines denote corresponding mirror planes of the $\mathcal{M}_x$, $\mathcal{M}_y$, $\mathcal{M}_{xy}$, and $\mathcal{M}_{x\bar{y}}$ symmetries. Edge spectra of the tight-binding model with an (b) out-of-plane ($\theta = 0^\circ$) and (c) in-plane magnetization ($\theta = 90^\circ$ and $\varphi = 45^\circ$) for the exchange field of $B = 0.5t$. (d) Energy spectrum of the 40×40 nanoflake of the model versus the magnitude of B. Corner states are highlighted with blue circles. Energy levels for a nanoflake with an (e) out-of-plane and (f) in-plane magnetization. Insets show the spatial weight of the edge states and corner states.

We first consider an out-of-plane FM ordering, $\theta = 0^\circ$. In this case, $\mathcal{M}_z$ remains intact with $\mathcal{M}_z^2 = -1$ while all other mirror symmetries and $\mathcal{T}$ are broken, meaning that the Hamiltonian can be separated into two decoupled mirror subspaces based on the two mirror eigenvalues $\pm i$:

$$H^{\pm i}(k_x, k_y) = \pm[m + B - t(\cos k_x + \cos k_y)]\sigma_z - \sin k_x \sigma_x \mp \sin k_y \sigma_y. \quad (2)$$

For two opposite mirror subspaces, the calculated Chern numbers are, respectively, $\mathcal{C}_{+i} = 1$ and $\mathcal{C}_{-i} = -1$. Thus, the mirror Chern number defined as $\mathcal{C}_\mathcal{M} = (\mathcal{C}_{+i} - \mathcal{C}_{-i})/2$ is $+1$, which proves the TCI nature of the considered 2D FM square lattice. This can be further explicitly confirmed by observing the emergence of gapless edge states at all edges with $\mathcal{M}_z$ as displayed in Figs. 1(b) and 1(e).

It is widely known that a gap opens up in the edge states when the protecting $\mathcal{M}_z$ symmetry is broken, for example by rotating the magnetic moments into the xy plane, $\theta = 90^\circ$. Indeed, our results reveal that the edges are usually gapped out in this case. However, for $\varphi = 0^\circ$ and $\varphi = 90^\circ$, $\mathcal{M}_x$ and $\mathcal{M}_y$ symmetries are still preserved, respectively, which keeps the edges, perpendicular to the corresponding mirror planes, gapless. Remarkably, for $\varphi = 45^\circ$, although the edges are gapped out [Fig. 1(c) with $B = 0.5t$], the in-gap states, that are localized in the corners of a finite sample, arise, as visible from the spectrum analysis of a 0D nanoflake in Fig. 1(f). This signals the emergence of the HOTI state. In the latter case the $\mathcal{M}_{xy}$ symmetry survives with the eigenvectors of $+i$ and $-i$ in corresponding subspaces, which can be written as $H_{\pm i} = q_{\pm i} \cdot \sigma$. Thus, a mirror-graded winding number, also known as Zak phase, can be calculated by $\nu_{\mathcal{M}_{xy}} = (\nu_{+i} - \nu_{-i})/2$ with

$$\nu_{\pm i} = \frac{i}{2\pi}\int_L dk\{\mathrm{Tr}[q_{\pm i}(k)\partial_k q_{\pm i}^{+}(k)]\}, \quad (3)$$

where the one-dimensional integration path L goes through Γ and follows the mirror-invariant (110) direction in the Brillouin zone. The calculated values of $\nu_{+i} = 1$ and $\nu_{-i} = -1$ result in a nonzero mirror-graded winding number $\nu_{\mathcal{M}_{xy}}$=1, confirming the fact that the HOTI can be obtained from the TCI via efficient magnetization switching in a 2D ferromagnet. The topological corner electrons are gradually accumulating as the Zeeman term increases, and they are found to localize in the corners exclusively when $B > 0.25t$ [Fig. 1(d)]. Moreover, since $\mathcal{P}$ is still preserved, we can also employ the parity eigenvalues analysis to examine the nontrivial topology by computing the winding number ν_{2D} defined

as [45,54]

$$(-1)^{\nu_{2D}} = \prod_{i=1}^{4} (-1)^{[N_{occ}^{-}(\Gamma_i)/2]}, \tag{4}$$

where $N_{occ}^{-}(\Gamma_i)$ is the number of occupied states with an odd parity at time-reversal invariant momenta Γ_i. As expected, we find that at the Γ point, the parity eigenvalues of two occupied states are all odd, whereas those for the other three momenta (two X and one M) are all even. This yields $\nu_{2D} = 1$ thus further explicitly confirming the HOTI state.

III. MATERIAL REALIZATION

Having demonstrated the generic physical mechanism of magnetization-driven transformation between a 2D FM TCI and a FM HOTI, we aim now at a material realization of a 2D intrinsic ferromagnet that exhibits the proposed quantum phase transition. Neptunium monopnictide NpSb has long been studied both theoretically and experimentally owing to its surprising electronic and magnetic properties [55–57] and was recently proposed to be an axion insulator [36]. Bulk NpSb crystallizes in the face-centered-cubic NaCl structure with space group $Fm\bar{3}m$ (No. 225), as shown in Fig. 2(a), where Np and Sb atoms occupy the Wyckoff 4*c* and 4*b* positions, respectively, and they are coplanar. Thus, when we construct a (001)-oriented monolayer of NpSb, a 2D square lattice with Np and Sb atoms positioned in the mirror plane $z = 0$ is obtained. Figure 2(c) presents the top view of such a 2D monolayer with the $p4/mmm$ (No. 61) layer group. We

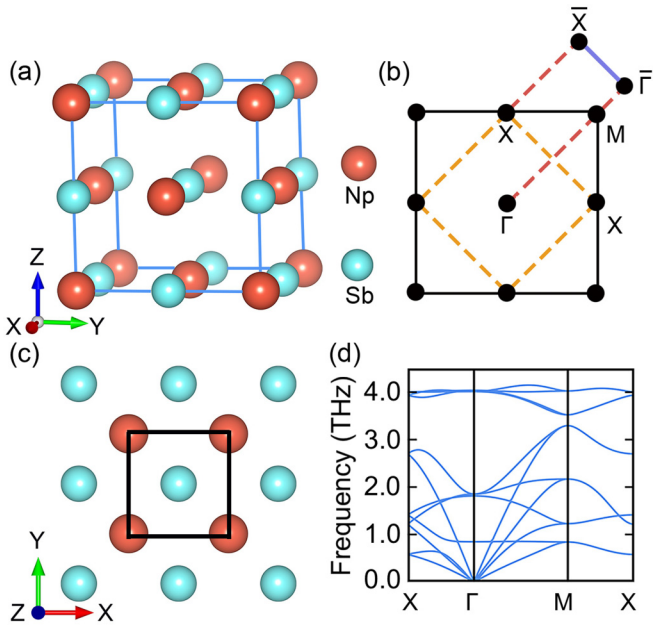

FIG. 2. Crystal structure of (a) bulk and (c) monolayer NpSb. The unit cell of NpSb monolayer is indicated by black solid lines. (b) The Brillouin zone of the primitive unit cell (black solid lines) and $\sqrt{2} \times \sqrt{2}$ supercell (yellow dashed lines) of the monolayer. Projected one-dimensional Brillouin zone with marked high symmetry points is shown with a purple solid line. (d) Phonon spectra for NpSb monolayer, indicating that the NpSb monolayer is dynamically stable.

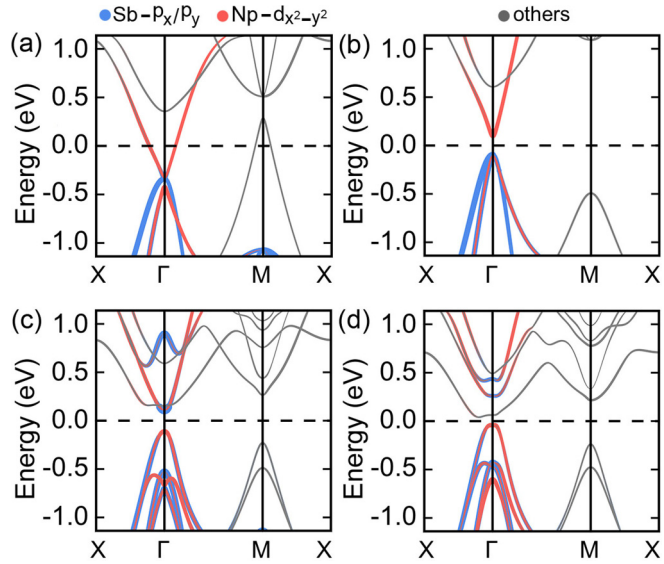

FIG. 3. Band structure of (a) majority and (b) minority states of NpSb monolayer in the absence of SOC, and that of NpSb monolayer with (c) an out-of-plane and (d) an in-plane magnetization along x including SOC. The bands are orbitally weighted with the contribution of Sb-$p_{x/y}$ and Np-$d_{x^2-y^2}$ states. The Fermi level is indicated with a dashed line.

refer to the Supplemental Material for the details of our first principles calculations which take into account the strongly-correlated nature of this material [53]. The determined from total energy calculations optimized lattice constant is $a = 4.41$ Å, almost the same as that of the experimental bulk structure [56]. Remarkably, as verified by our explicit calculations of the phonon spectrum, plotted in Fig. 2(d), all phonon branches are positive in the entire Brillouin zone, which signifies that NpSb monolayer is dynamically stable and difficult to destroy once formed.

The ground state of NpSb monolayer was found to be FM and the corresponding band structure of the system without SOC is illustrated in Figs. 3(a) and 3(b). Clearly, the majority bands are metallic with a band touching at the Γ point, while the minority bands exhibit a gap of 195 meV resulting in a pronounced half-metallic behavior near the Fermi energy. We next inspect the effect of SOC on the band structure and present the data in Figs. 3(c) and 3(d) for the out-of-plane and in-plane (along x) directions of the magnetization. As can be seen from this figure, SOC opens a very large gap in the majority channel, thereby making the whole system gapped for both directions of the magnetization, with the corresponding band gaps constituting 220 meV and 86 meV for the out-of-plane and in-plane directions, respectively. Moreover, the fat-band analysis of the orbital contributions to the electronic states suggests that SOC drives a band inversion between Sb-p_x/p_y and Np-$d_{x^2-y^2}$ states both in the minority and majority channels. As is well known, such a band inversion is a clear indicator of the formation of a topologically nontrivial insulator.

For the out-of-plane magnetization, the magnetic space group [58,59] of such a system is $P4/mm'm'$ (No. 123.345) with one Np and one Sb atom occupying the Wyckoff 1*b* and 1*d* positions, respectively, where the magnetic moment

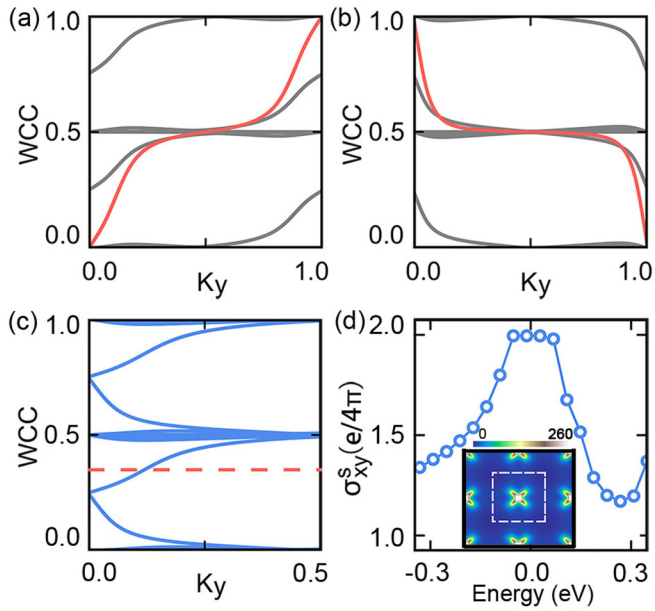

FIG. 4. Evolution of Wannier charge centers (WCCs) for NpSb monolayer with an out-of-plane magnetization associated with (a) $+i$ and (b) $-i$ mirror eigenstates, indicating a nonzero mirror Chern number $\mathcal{C}_{\mathcal{M}} = 1$. (c) Evolution of WCCs along k_x, confirming the topological nature of the gap with $\mathbb{Z}_2 = 1$. (d) Energy dependence of the spin Hall conductivity σ^S_{xy}, showing a quantized value within the energy window of the SOC gap. Inset shows the reciprocal-space distribution of spin Berry curvature within the SOC gap.

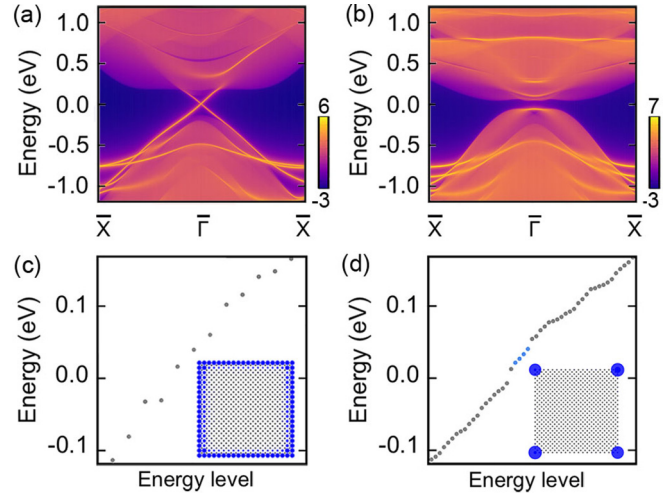

FIG. 5. Energy bands of the semi-infinite NpSb nanoribbon with (a) out-of-plane and (b) in-plane ferromagnetism, revealing characteristic edge states for the TCI and HOTI phases, respectively. Colors range from purple to red representing the higher density of states at the edges. Energy levels for a NpSb nanoflake with the (c) out-of-plane and (d) in-plane ferromagnetism. Corner states in (d) are highlighted in blue circles. Insets show the probability of the edge states and corner states.

is only on Np atom with an amplitude of $4\mu_B$. In this magnetic space group, the system possesses $\mathcal{M}_z$ symmetry, and thus, all Bloch states can be distinguished by their mirror eigenvalues $\pm i$, while the mirror Chern number $\mathcal{C}_{\mathcal{M}}$ can be assessed. In order to do this, we construct a tight-binding Hamiltonian based on the maximally localized Wannier functions and for each value of k_y carry out the Wilson loop calculations, where the Wilson loop matrix is determined as $W_{(k_x+2\pi,k_y)\leftarrow(k_x,k_y)} = \lim_{N\to\infty} F_{N-1}F_{N-2}\ldots F_1F_0$, where $[F_i]_{mn} = \langle u_m(2\pi(i+1)/N, k_y) \mid u_n(2\pi i/N, k_y)\rangle$, with $|u_{n\mathbf{k}}\rangle$ as the lattice-periodic part of the nth Bloch state at the k point (k_x, k_y), N is the number of k_x points we set, and the dimension of the Wilson loop matrix is equal to the number of occupied bands of our system. As shown in Figs. 4(a) and 4(b), the Chern numbers of all occupied bands for the opposite mirror eigenvalues $+i$ and $-i$ are $\mathcal{C}_{+i} = 1$ and $\mathcal{C}_{-i} = -1$, respectively, yielding $\mathcal{C}_{\mathcal{M}} = 1$, and confirming the fact that NpSb monolayer is a 2D FM TCI. In addition, to further solidify the nontrivial topology with an odd number of band inversions, the $\mathbb{Z}_2$ invariant is calculated through both the Wannier charge centers (WCCs) and the spin Hall conductivity σ^S_{xy}. An odd number of crossings of the WCCs with a reference horizontal line and the quantization of σ^S_{xy} within the insulating region are clearly visible, as shown in Figs. 4(c) and 4(d), uncovering that the topological index $\mathbb{Z}_2$ is $+1$ and implying the quantum spin Hall nature of our 2D FM system. Therefore, the NpSb monolayer exhibits the dual topological character with respect to the 2D FM TCI and FM quantum spin Hall effect.

Now, we turn to the NpSb monolayer with an in-plane magnetization along (100) and validate the emergence of 2D HOTI phase. The magnetic space group [58,59] turns into $Cmm'm'$ (No. 65.486) with both Np and Sb atoms at its Wyckoff 2d positions, who shares the same amplitude of magnetic moment as out-of-plane magnetization. Although the obtained band structure for the in-plane magnetization differs somewhat from that obtained for the out-of-plane case, as shown in Figs. 3(c) and 3(d), the SOC-driven band inversion between the valence and conduction bands is preserved. Thus, the occupied states at four time-reversal invariant momenta (one Γ, two X, and one M) still retain their parity eigenvalues. There are 14, 8, and 16 odd bands out of 20 occupied bands at Γ, X, and M, respectively. Therefore the parities at (Γ, X_1, X_2, M) are $(-, +, +, +)$, which leads to $\nu_{2D} = 1$, thus revealing the existence of the FM HOTI phase in the NpSb monolayer.

Finally, we investigate the emergence of edge and corner states in our system, which are the hallmarks of 2D TCIs and HOTIs, using the maximally localized Wannier functions that can reproduce the band dispersion of FM NpSb for the out-of-plane and in-plane directions of the magnetization very accurately. Figures 5(a) and 5(b) display the edge spectra for the semi-infinite along (100) NpSb. One can clearly observe that, in direct agreement with $\mathcal{C}_{\mathcal{M}} = 1$ prediction for the out-of-plane case, a pair of counterpropagating gapless edge states meets at the Γ point, Fig. 5(a). In contrast, the edge states become completely gapped for the in-plane magnetization direction due to the $\mathcal{M}_z$ symmetry breaking [Fig. 5(b)]. Notably, the topological corner states arise around the Fermi level as illustrated by the calculation of the energy levels of a 20×20 0D nanoflake plotted in Fig. 5(d). Inset of Fig. 5(d) presents the corresponding real-space distribution of the states. Indeed, with fractionalized charge distribution, wave functions of the corner states are localized only at the corners shared by

adjacent boundaries, whereas the corner states essentially vanish in other regions. This is topologically distinct from the edge states exhibited in the dual TI state of the system, as shown in the inset of Fig. 5(c), where the edge states are clearly visible to be distributed almost uniformly along the boundaries. These results unambiguously demonstrate the realization of the 2D FM TCI and HOTI phases in the NpSb monolayer as controlled by the direction of the magnetization.

IV. CONCLUSIONS

In conclusion, we have demonstrated the emergence of a FM TCI and FM HOTI phases for a magnet on a 2D square lattice, which can be controlled by switching the magnetization direction, e.g., via electrically induced spin-orbit torques, providing thus a promising way to control the symmetry and the state of magnetic systems which host higher-order topology. Moreover, we identified NpSb monolayer as an ideal platform for achieving the proposed magnetic topologies. It possesses the required magnetic group symmetry and stable crystal structure. The FM TCI state for an out-of-plane magnetization is identified by a mirror Chern number $\mathcal{C}_{\mathcal{M}} = 1$ and a pair of gapless edge states, while the FM HOTI state for an in-plane magnetization is identified by the index $\nu_{2D} = 1$ and corner states. Our findings may motivate the formulation of novel strategies in manipulating topological phenomena and exotic topological states for spintronics applications.

ACKNOWLEDGMENTS

This work is supported by the National Natural Science Foundation of China (Grants No. 11904205 and No. 12074217), the Shandong Provincial Natural Science Foundation (Grants No. ZR2019QA019 and No. ZR2019MEM013), the Shandong Provincial Key Research and Development Program (Major Scientific and Technological Innovation Project) (Grant No. 2019JZZY010302), Taishan Scholar Program of Shandong Province, and Qilu Young Scholar Program of Shandong University. The work was also supported by the Deutsche Forschungsgemeinschaft (DFG, German Research Foundation) — TRR 288 - 422213477 (Project No. A06), and Sino-German Project DISTOMAT (MO 1731/10-1).

[1] L. Fu, Phys. Rev. Lett. **106**, 106802 (2011).
[2] T. H. Hsieh, H. Lin, J. Liu, W. Duan, A. Bansil, and L. Fu, Nat. Commun. **3**, 982 (2012).
[3] C.-H. Hsu, X. Zhou, T.-R. Chang, Q. Ma, N. Gedik, A. Bansil, S.-Y. Xu, H. Lin, and L. Fu, Proc. Natl. Acad. Sci. USA **116**, 13255 (2019).
[4] C.-H. Hsu, X. Zhou, Q. Ma, N. Gedik, A. Bansil, V. M. Pereira, H. Lin, L. Fu, S.-Y. Xu, and T.-R. Chang, 2D Mater. **6**, 031004 (2019).
[5] T. Zhang, C. Yue, T. Zhang, S. Nie, Z. Wang, C. Fang, H. Weng, and Z. Fang, Phys. Rev. Research **1**, 012001(R) (2019).
[6] X.-L. Qi and S.-C. Zhang, Rev. Mod. Phys. **83**, 1057 (2011).
[7] M. Z. Hasan and C. L. Kane, Rev. Mod. Phys. **82**, 3045 (2010).
[8] A. Bansil, H. Lin, and T. Das, Rev. Mod. Phys. **88**, 021004 (2016).
[9] Y. Ando and L. Fu, Annu. Rev. Condens. Matter Phys. **6**, 361 (2015).
[10] C. Fang and L. Fu, Phys. Rev. B **91**, 161105(R) (2015).
[11] Y. Tanaka, Z. Ren, T. Sato, K. Nakayama, S. Souma, T. Takahashi, K. Segawa, and Y. Ando, Nat. Phys. **8**, 800 (2012).
[12] P. Dziawa, B. J. Kowalski, K. Dybko, R. Buczko, A. Szczerbakow, M. Szot, E. Łusakowska, T. Balasubramanian, B. M. Wojek, M. H. Berntsen, O. Tjernberg, and T. Story, Nat. Mater. **11**, 1023 (2012).
[13] S.-Y. Xu, C. Liu, N. Alidoust, M. Neupane, D. Qian, I. Belopolski, J. D. Denlinger, Y. J. Wang, H. Lin, L. A. Wray, G. Landolt, B. Slomski, J. H. Dil, A. Marcinkova, E. Morosan, Q. Gibson, R. Sankar, F. C. Chou, R. J. Cava, A. Bansil *et al.*, Nat. Commun. **3**, 1192 (2012).
[14] J. Liu, T. H. Hsieh, P. Wei, W. Duan, J. Moodera, and L. Fu, Nat. Mater. **13**, 178 (2014).
[15] E. O. Wrasse and T. M. Schmidt, Nano Lett. **14**, 5717 (2014).
[16] J. Liu, X. Qian, and L. Fu, Nano Lett. **15**, 2657 (2015).
[17] C. Niu, P. M. Buhl, G. Bihlmayer, D. Wortmann, S. Blügel, and Y. Mokrousov, Nano Lett. **15**, 6071 (2015).
[18] C. Niu, P. M. Buhl, G. Bihlmayer, D. Wortmann, Y. Dai, S. Blügel, and Y. Mokrousov, Phys. Rev. B **95**, 075404 (2017).
[19] M. Eschbach, M. Lanius, C. Niu, E. Młyńczak, P. Gospodarič, J. Kellner, P. Schüffelgen, M. Gehlmann, S. Döring, E. Neumann, M. Luysberg, G. Mussler, L. Plucinski, M. Morgenstern, D. Grützmacher, G. Bihlmayer, S. Blügel, and C. M. Schneider, Nat. Commun. **8**, 14976 (2017).
[20] Y. Xu, Z. Song, Z. Wang, H. Weng, and X. Dai, Phys. Rev. Lett. **122**, 256402 (2019).
[21] C. Fang, M. J. Gilbert, and B. A. Bernevig, Phys. Rev. Lett. **112**, 046801 (2014).
[22] C. Niu, P. M. Buhl, G. Bihlmayer, D. Wortmann, S. Blügel, and Y. Mokrousov, Phys. Rev. B **91**, 201401(R) (2015).
[23] C. Niu, J.-P. Hanke, P. M. Buhl, H. Zhang, L. Plucinski, D. Wortmann, S. Blügel, G. Bihlmayer, and Y. Mokrousov, Nat. Commun. **10**, 3179 (2019).
[24] N. Mao, X. Hu, C. Niu, B. Huang, and Y. Dai, Phys. Rev. B **100**, 205116 (2019).
[25] J. Li, Y. Li, S. Du, Z. Wang, B.-L. Gu, S.-C. Zhang, K. He, W. Duan, and Y. Xu, Sci. Adv. **5**, eaaw5685 (2019).
[26] D. Zhang, M. Shi, T. Zhu, D. Xing, H. Zhang, and J. Wang, Phys. Rev. Lett. **122**, 206401 (2019).
[27] M. M. Otrokov, I. P. Rusinov, M. Blanco-Rey, M. Hoffmann, A. Y. Vyazovskaya, S. V. Eremeev, A. Ernst, P. M. Echenique, A. Arnau, and E. V. Chulkov, Phys. Rev. Lett. **122**, 107202 (2019).
[28] H. Sun, B. Xia, Z. Chen, Y. Zhang, P. Liu, Q. Yao, H. Tang, Y. Zhao, H. Xu, and Q. Liu, Phys. Rev. Lett. **123**, 096401 (2019).
[29] C. Niu, H. Wang, N. Mao, B. Huang, Y. Mokrousov, and Y. Dai, Phys. Rev. Lett. **124**, 066401 (2020).

[30] N. Mao, H. Wang, X. Hu, C. Niu, B. Huang, and Y. Dai, Phys. Rev. B **102**, 115412 (2020).

[31] H. Wang, N. Mao, X. Hu, Y. Dai, B. Huang, and C. Niu, Mater. Horizons **8**, 956 (2021).

[32] H. Wang, N. Mao, C. Niu, S. Shen, M.-H. Whangbo, B. Huang, and Y. Dai, Mater. Horizons **7**, 2431 (2020).

[33] H. Li, S.-Y. Gao, S.-F. Duan, Y.-F. Xu, K.-J. Zhu, S.-J. Tian, J.-C. Gao, W.-H. Fan, Z.-C. Rao, J.-R. Huang *et al.*, Phys. Rev. X **9**, 041039 (2019).

[34] Y.J. Chen, L. X. Xu, J. H. Li, Y. W. Li, H. Y. Wang, C. F. Zhang, H. Li, Y. Wu, A. J. Liang, C. Chen, S. W. Jung, C. Cacho, Y. H. Mao, S. Liu, M. X. Wang, Y. F. Guo, Y. Xu, Z. K. Liu, L. X. Yang, and Y. L. Chen, Phys. Rev. X **9**, 041040 (2019).

[35] S. Zhang, R. Wang, X. Wang, B. Wei, B. Chen, H. Wang, G. Shi, F. Wang, B. Jia, Y. Ouyang *et al.*, Nano Lett. **20**, 709 (2019).

[36] Y. Xu, L. Elcoro, Z. D. Song, B. J. Wieder, M. G. Vergniory, N. Regnault, Y. Chen, C. Felser, and B. A. Bernevig, Nature (London) **586**, 702 (2020).

[37] W. A. Benalcazar, B. A. Bernevig, and T. L. Hughes, Science **357**, 61 (2017).

[38] F. Schindler, A. M. Cook, M. G. Vergniory, Z. Wang, S. S. Parkin, B. A. Bernevig, and T. Neupert, Sci. Adv. **4**, eaat0346 (2018).

[39] F. Schindler, Z. Wang, M. G. Vergniory, A. M. Cook, A. Murani, S. Sengupta, A. Y. Kasumov, R. Deblock, S. Jeon, I. Drozdov, H. Bouchiat, S. Guéron, A. Yazdani, B. A. Bernevig, and T. Neupert, Nat. Phys. **14**, 918 (2018).

[40] C. W. Peterson, W. A. Benalcazar, T. L. Hughes, and G. Bahl, Nature (London) **555**, 346 (2018).

[41] M. Serra-Garcia, V. Peri, R. Süsstrunk, O. R. Bilal, T. Larsen, L. G. Villanueva, and S. D. Huber, Nature (London) **555**, 342 (2018).

[42] S. Imhof, C. Berger, F. Bayer, J. Brehm, L. W. Molenkamp, T. Kiessling, F. Schindler, C. H. Lee, M. Greiter, T. Neupert, and R. Thomale, Nat. Phys. **14**, 925 (2018).

[43] Z. Wang, B. J. Wieder, J. Li, B. Yan, and B. A. Bernevig, Phys. Rev. Lett. **123**, 186401 (2019).

[44] C. Yue, Y. Xu, Z. Song, H. Weng, Y. M. Lu, C. Fang, and X. Dai, Nat. Phys. **15**, 577 (2019).

[45] M. J. Park, Y. Kim, G. Y. Cho, and S. B. Lee, Phys. Rev. Lett. **123**, 216803 (2019).

[46] R.-X. Zhang, F. Wu, and S. Das Sarma, Phys. Rev. Lett. **124**, 136407 (2020).

[47] C. W. Peterson, T. Li, W. A. Benalcazar, T. L. Hughes, and G. Bahl, Science **368**, 1114 (2020).

[48] B. Liu, G. Zhao, Z. Liu, and Z. F. Wang, Nano Lett. **19**, 6492 (2019).

[49] X.-L. Sheng, C. Chen, H. Liu, Z. Chen, Z.-M. Yu, Y. X. Zhao, and S. A. Yang, Phys. Rev. Lett. **123**, 256402 (2019).

[50] E. Lee, R. Kim, J. Ahn, and B. J. Yang, npj Quantum Mater. **5**, 1 (2020).

[51] Y. Ren, Z. Qiao, and Q. Niu, Phys. Rev. Lett. **124**, 166804 (2020).

[52] C. Chen, Z. Song, J.-Z. Zhao, Z. Chen, Z.-M. Yu, X.-L. Sheng, and S. A. Yang, Phys. Rev. Lett. **125**, 056402 (2020).

[53] See Supplemental Material for http://link.aps.org/supplemental/10.1103/PhysRevB.103.195152 details of the first-principles calculations and additional results of the tight-binding model, which includes Refs. [60–66].

[54] J. Ahn, D. Kim, Y. Kim, and B.-J. Yang, Phys. Rev. Lett. **121**, 106403 (2018).

[55] M. Amanowicz, D. Braithwaite, V. Ichas, U. Benedict, J. Rebizant, and J. C. Spirlet, Phys. Rev. B **50**, 6577 (1994).

[56] D. Jones, W. Stirling, G. Lander, J. Rebizant, J. Spirlet, M. Alba, and O. Vogt, J. Phys.: Condens. Matter **3**, 3551 (1991).

[57] V. Ichas, S. Zwirner, D. Braithwaite, J. C. Spirlet, J. Rebizant, and W. Potzel, Phys. Rev. B **56**, 14481 (1997).

[58] M. I. Aroyo, J. M. Perez-Mato, C. Capillas, E. Kroumova, S. Ivantchev, G. Madariaga, A. Kirov, and H. Wondratschek, Z. Kristallogr. Cryst. Mater. **221**, 15 (2006).

[59] J. Perez-Mato, S. Gallego, E. Tasci, L. Elcoro, G. de la Flor, and M. Aroyo, Annu. Rev. Mater. Sci. **45**, 217 (2015).

[60] J. P. Perdew, K. Burke, and M. Ernzerhof, Phys. Rev. Lett. **77**, 3865 (1996).

[61] G. Kresse and J. Furthmüller, Phys. Rev. B **54**, 11169 (1996).

[62] See http://www.flapw.de.

[63] A. A. Mostofi, J. R. Yates, Y.-S. Lee, I. Souza, D. Vanderbilt, and N. Marzari, Comput. Phys. Commun. **178**, 685 (2008).

[64] F. Freimuth, Y. Mokrousov, D. Wortmann, S. Heinze, and S. Blügel, Phys. Rev. B **78**, 035120 (2008).

[65] Q. Wu, S. Zhang, H.-F. Song, M. Troyer, and A. A. Soluyanov, Comput. Phys. Commun. **224**, 405 (2018).

[66] A. Togo and I. Tanaka, Scr. Mater. **108**, 1 (2015).